scientific reports

Check for updates

OPEN

Insights into the pharmaceutical properties of green fabricated Iron oxide nanoparticles

H. N. K. AL-Salman[1], Qutaiba A. Qasim[2], Basil A. Abbas[3], Adel J. Hussein[3], Falah Hassan Shari[4], Majid S. Jabir[5]✉, Mansour K. Gatasheh[6]✉, Ammar AL-Farga[7] & Hayder Adnan Fawzi[8]✉

Researchers have recently grown interested in utilizing plant extracts as effective reducing agents for the eco-friendly synthesis of nanoparticles. The present investigation involved the preparation of Iraqi onion extract (*Allium cepa*), which was further utilized as a reducing agent for the biosynthesis of Fe_3O_4-nanoparticles (NPs). Characterization of nanoparticles was conducted using UV-visible spectroscopy, TEM, XRD, FT-IR, FESEM, and EDS analyses. The in vitro cytotoxicity was assessed in MDCK-SIAT cells utilizing the MTT assay, while the antiviral efficacy was examined with the neuraminidase assay kit MAK12. Antibacterial efficacy was examined against *S. aureus* and *E.* coli utilizing a disk-diffusion methodology. The DPPH assay was employed to evaluate antioxidant activity. The impact of *A. cepa* extract and Fe_3O_4-NPs on phagocytic cell activity was evaluated. Our findings demonstrated the production of solid, crystalline, semi-spherical Fe_3O_4 measuring 36 ± 1.23 nm, exhibiting significant antibacterial, antiviral, and antioxidant properties. *A. cepa* extract and Fe_3O_4-NPs can augment the phagocytic activity of phagocytic cells by elevating the formation of reactive oxygen species. In conclusion, Onion peel extract is a superior option for synthesizing Fe_3O_4-NPs, which may be employed in many therapeutic applications in the future.

Keywords Onion peel extract, Iron oxide nanoparticles, Bactericidal, Antioxidant, Phagocytosis, Green synthesis

Fe_3O_4-nanoparticles (NPs) are commonly utilized throughout several industries, including chemical, medicinal, and agricultural activities, owing to their distinctive properties, particularly their robust magnetization[1–3]. Recent research indicates that Fe_3O_4-NPs possess significant promise for biomedical applications, including targeted medication and gene delivery, antibacterial anticancer, tissue engineering[4–6]. Diverse synthesis procedures for Fe3O4 nanoparticles, including sol-gel, coprecipitation, solvothermal, and hydrothermal methods, have been utilized to produce nanoparticles with desired characteristics[7–11]. The utilization of dangerous chemicals, elevated manufacturing expenses, and the generation of undesired byproducts are all disadvantages of these methods[12].

Investigation into green synthesis methodologies is increasingly important to address the issues caused by standard procedures[13,14]. Green synthesis has numerous advantages, such as simplicity of application, rapid manufacturing processes, reduced production costs, and minimized waste generation[15]. The ecosystem and human health are seriously threatened by the presence of heavy metals, dyes, and antibiotics in wastewater or effluent. Metallic nanoparticles have been effectively used to detect and eliminate heavy metals, dyes, and antibiotics[16]. The green chemistry procedure is followed in the green synthesis of metallic nanoparticles. It is an economical and environmentally responsible way to get NPs. Plant-mediated synthesis is becoming more and more popular among greener techniques for the creation of metallic nanoparticles[16,17].

[1]Department of Pharmaceutical Chemistry, College of Pharmacy, University of Basrah, Basrah, Iraq. [2]College of Pharmacy, Al-Ayen University, Dhi Qar, Iraq. [3]Department of Microbiology, College of Veterinary Medicine, University of Basrah, Basrah, Iraq. [4]Department of Clinical Laboratory Sciences, College of Pharmacy, University of Basrah, Basrah, Iraq. [5]Department of Applied Sciences, University of Technology, Baghdad, Iraq. [6]Department of Biochemistry, College of Science, King Saud University, P.O. Box-2455, Riyadh 11451, Saudi Arabia. [7]State Key Laboratory of Food Science and Technology, Jiangnan University, Wuxi 214122, Jiangsu, China. [8]Department of Clinical Pharmacy, College of Pharmacy, AlMustafa University, Baghdad, Iraq. ✉email: 100131@uotechnology.edu.iq; mgatasheh@ksu.edu.sa; hayder.adnan2010@gmail.com

Researchers are presently focused on the latest developments in nanotechnology and biosynthetic methods utilizing plant extracts due to the beneficial combination between natural products and the characteristics of the resulting nanostructures, which can serve as effective alternatives for various applications in an environmentally sustainable manner[18]. The perennial herb, *Allium cepa*, namely the Iraqi onion, belonging to the Amaryllidaceae family, is among the most recognized and commonly utilized seasoning plants[19].

It possesses distinctive therapeutic characteristics due to its substantial content of phenolic compounds, magnesium, vitamin B6, phosphorus, folic acid, calcium, potassium, other vitamins and minerals, minimal fat, and certain amino acids, such as arginine and glutamic acid[20]. Onion species are widely utilized in both conventional and alternative therapies for various conditions, including digestive system disorders, respiratory infections, and cardiovascular diseases, owing to the bioactive compounds present in onion extract that exhibit anti-inflammatory, antibacterial, antioxidant, and immunomodulatory properties[21–24]. Allium species serve as excellent reducing compounds and have been utilized for the green synthesis of various metal nanoparticles[25–27].

Limited research exists on the green fabrication of Fe3O4 nanoparticles utilizing Allium species extract and their application in the biomedical sector. This study seeks to produce Fe3O4 nanoparticles using a sustainable approach with A. cepa peel extract, define their structural properties, and assess their effectiveness in antibacterial and antiviral activities, antioxidant capacity, and as phagocytosis inducers.

Methods

Chemical and materials

Chloride hexahydrate ($FeCl_3{\cdot}6H_2O$), Chloride tetrahydrate ($FeCl_2{\cdot}4H_2O$), and sodium hydroxide (NaOH) were acquired from Sigma-Aldrich Pty Ltd in Darmstadt, Germany. Peels of *Allium cepa* were procured at the local market in Basrah, Iraq. The bacterial strains *Escherichia coli* and *Staphylococcus aureus* were provided by the Microbiology Research Laboratory of Basrah University.

Extraction

Professor Dr Mohammad A.H. Alnajjar authenticated the plant in the Department of Horticulture and Landscape, College of Agriculture, University of Basrah, Iraq, a collection of *Allium cepa* peels. A voucher specimen was deposited in the scientific affairs of the University of Basrah, College of Agriculture.

A precise amount of onion peels (20 g) was thoroughly cleaned with distilled water, boiled in 200 mL of water for 50 min, thereafter filtered, and stored in a cool environment (4℃) for use as a reducing agent in the biosynthesis of Fe_3O_4 nanoparticles.

Preparation of iron oxide nanoparticles

The synthesis method was executed as follows: a mixture of $FeCl_3.6H_2O$ and $FeCl_2.4H_2O$ in a 2:1 molar ratio was introduced to a specified volume of *A. cepa* extract to yield a brown colloidal solution, after which 1.0 M NaOH was incrementally introduced while the solution was continuously agitated. The pH of the mixture was modified to 11. Subsequently, the mixture was agitated for one hour to achieve homogeneity and to complete the reaction. A permanent magnet was subsequently employed to isolate the synthesized Fe_3O_4 nanoparticles. Deionized water was employed to wash the Fe_3O_4 nanoparticles repeatedly. The nanoparticles were dehydrated in an oven maintained at around 72℃ for one day. The desiccated material was stored in a hermetically sealed container for further investigation. All trials were conducted at ambient temperature[28].

Characterization of Fe_3O_4-NPs

XRD analysis was employed to ascertain the presence and phase purity of the synthesized Fe_3O_4-NPs[29]. The dry sample underwent CuK radiation ($\lambda = 1.54$ nm) in a 2-angle arrangement, scanning from 5° to 80° at a rate of 2°/min, with an applied current of 20 mA and an accelerating voltage of 45 kV. The Shimadzu UV-Visible Spectrophotometer (UV-1800) was employed to ascertain the UV-Vis spectra of Fe_3O_4-NPs. A Fourier-transform infrared spectrophotometer (FTIR) (Bruker, Germany) was employed to capture the spectra. The dimensions and morphology of the synthesized Fe_3O_4-NPs were examined via TEM (ZEISS LEO 912, Oberkochen, Germany) at an accelerating voltage of 100 kV. The elemental composition of the samples was examined using energy-dispersive field emission scanning electron microscopy (FESEM). The synthesized Fe_3O_4-NPs was optimized according to the studies by Win et al.[28].

Cytotoxicity assays (MTT assay)

The MTT experiments were conducted in 96-well plates to assess the cytotoxicity of Fe_3O_4-NPs. Each well of the dish was inoculated with a quantity of 104 MDCK cells. After 24 h, upon the formation of a confluent monolayer in the cells, varying quantities of *A. cepa* and Fe_3O_4-NPs (25–100 µg/ml) were introduced to the cell culture. Following a 48-hour period, the medium was removed and substituted with 100 µL of a 2 mg/mL MTT solution, incubated for 2.5 h at 37 ℃. The vitality of the cells was subsequently evaluated. The MTT solution was discarded, and 130 µL of dimethyl sulfoxide (DMSO) was added for 15 min. The absorbance was recorded three times using a microplate reader at a wavelength of 492 nm[30–32].

Viral infection

The infectivity of influenza A in MDCK-SIAT1 cells was assessed utilizing Tris-EDTA buffer and 20% DMSO as controls. In the aforementioned media, triplicate cell cultures comprising 1×10^4 cells were maintained for 24 h. In the final phase, a multiplicity of infection (MOI) of 0.1 was employed to infect the cells. After 48 h, the virus was eliminated from the cells by a procedure referred to be double optimum washing. Subsequently, the MTT tetrazolium reduction assay was conducted to assess cell viability. Three distinct sets of tests were conducted under identical conditions.

Antiviral activity

We employed the Neuraminidase Assay Kit MAK121 to assess the antiviral efficacy in MDCK-SIAT1 cells infected with Influenza A, utilizing Oseltamivir as a positive experimental control (Sigma-Aldrich; St Louis, MO, USA). The 96-well plates containing 1×10^4 cells were pretreated with A. cepa extract and Fe_3O_4 nanoparticles at 25 to 100 µg/ml doses for one hour. Subsequently, the cells were removed by a two-step medium renewal procedure, followed by incubation with the virus at a multiplicity of infection (MOI) of 0.1 for 60 min. Following 48 h of infection, virus particles were eradicated using neutralizing antibodies, and the quantity of fresh virus was assessed by quantifying neuraminidase activity[32,33].

Antibacterial activity of *A. cepa* extract and Fe_3O_4-NPs

The antibacterial efficacy was examined utilizing the agar well diffusion technique[34,35], which was evaluated against *E. coli* and *Staphylococcus aureus*. Prior to initiating the culturing procedure, approximately 20 mL of Mueller-Hinton (M-H) was aseptically dispensed into sterile Petri dishes. Employing a sterile wire loop, we were able to isolate distinct bacterial species from their stock cultures. Wells were created in the agar plates using a sterile tip to form a well measuring 6 mm in diameter as the final step in the cultivation of the organisms[36]. Seventy-five microliters from various concentrations (0, 100, 150, 200, 250, and 300 µg/ml) of *A. cepa extract* and Fe_3O_4-NPs were introduced into the wells. The plates were incubated at 37℃ for 24 h. The mean diameter of the bacterial inhibition zones produced by the different concentrations was measured and documented[37].

Assessment of bacterial cells' viability

The Acridine orange/ethidium bromide (AO/EtBr) staining procedure is utilized to differentiate the bacterial cell viability following treatment with *A. cepa* extract and Fe_3O_4-NPs at a concentration of 150 µg/ml. The vitality of bacterial strains is assessed using a fluorescence microscope. Fifty microliters of the bacterial suspension were combined with fifty microliters of AO/EtBr at a concentration of 10 µg/ml for 120 s. Live cells stained with acridine orange exhibit green fluorescence, but dead cells labeled with ethidium bromide display red fluorescence.

Assay for ROS generation

A flow cytometry experiment was used to measure the generation of reactive oxygen species in bacterial cells after being treated with *A. cepa* extract and Fe_3O_4-NPs at a concentration of 150 µg/ml. Briefly, *A. cepa* extract and Fe_3O_4-NPs at a concentration of 150 µg/ml were exposed to *S. aureus* and *E. coli* for 12 h at 37 °C. Centrifugation was then used to harvest the cells. Using PBS buffer, a homogeneous solution of up to 1 ml was made from the cell pellet. As a result, the cells were incubated at 37 °C for 30 min with 1.5 ml of 100 µM DCFH2-DA. Flow cytometry (FACSVerse) was used to analyze the generation of ROS.

Change in membrane potential

Rhodamine-123 (Rh123) dye was used to measure the depolarization of the bacterial membrane. *A. cepa* extract and Fe_3O_4-NPs at a concentration of 150 µg/ml were applied to *S. aureus* and *E. coli* for 24 h at 37 °C. Centrifugation was then used to harvest the bacterial cells. After removing the cell pellet, PBS buffer was used to create a homogeneous solution up to 1 ml. The cell suspension was mixed with Rh123 dye, and the samples were kept in the dark for ten minutes. Flow cytometry (FACSVerse) to assess the results.

DPPH assay

DPPH was mixed with different concentrations of *A. cepa* extract and prepared Fe_3O_4-NPs (25, 50, 100, 200 µg/mL) incubated in the dark for 30 min. Following the equation below, the Fe_3O_4-NPs radical scavenging activity was tested by recording the DPPH radical absorbance at 515 nm.

$$Radical\ \ Scavenging\ \ activity\ \ = \frac{OD_{Control} - OD_{Sample}}{OD_{Control}} \times 100$$

ABTS assay

ABTS-activated radicals were generated by combining an ABTS solution with equal volumes of ABTS (7 mM) and potassium persulfate (2.45 mM) solutions. The diluted ABTS standard solution was introduced following a 12-hour incubation in darkness at 25℃, and the absorbance of the ABTS radical (0.7) at 734 nm was recorded. Ultimately, 5 µL of *A. cepa* extract and synthesized Fe_3O_4-NPs at several concentrations (25, 50, 100, and 200 µg/mL) were combined with 3.995 mL of the ABTS standard solution and incubated for 20 min. The radical scavenging activity was evaluated by measuring the absorbance of ABTS radicals at 734 nm.

Assessment of the phagocytic activity

BMDMs were isolated and seeded at a concentration of 4×10^5 in 6-well plates. Cells were treated with *A. cepa* extract and prepared Fe_3O_4-NPs at 25 µg/ml concentration for 24 h. *Candida albicans* at a ratio of 1:5 were incubated with BMDMs for 60 min and stained with methylene blue at a concentration of 0.5%. Cells were observed and counted; the blue cells were inactive, and the transparent ones were active. Results were expressed as phagocytosis index (PI).

Phagocytosis of pH_{rodo} *E. coli* bioparticles by BMDMs

BMDMs were seeded in a 4-well plate; they were pre-treated with *A. cepa* extract and prepared Fe_3O_4-NPs at 25 µg/ml. After adding 100 µl of pH_{rodo} *E. coli* particles, a buffer solution (100 µl) was added to them for 2 h. Cells were fixed, and a flow cytometry assay was used to read the results.

Statistical analysis

The one-way ANOVA or two-way ANOVA used to analyze the results, Graph Pad Prism 10.4, was employed[38]. Data presented as mean ± standard deviation (all experiments conducted in triplicate)[39].

Results

Characterization

The phase purity and crystallinity of the produced Fe3O4-NPs can be assessed by XRD analysis. Figure 1A illustrates the XRD patterns of green-synthesized Fe3O4 nanoparticles. The crystal planes (200, 311, 400, 422, 511, 440, and 533 correspond to the diffraction peaks of synthesized Fe_3O_4-NPs at 2θ values of 30.26°, 35.82°, 43.34°, 53.38°, 57.18°, 62.56°, and 72.48°, respectively. The XRD corresponded with JCPDS file No. 79–0417 for Fe_3O_4-NPs; their cubic crystalline system aligned well with the analyzed diffraction peaks. A noticeable color change and UV-Vis spectrum measurement confirmed the formation of Fe_3O_4 nanoparticles.

The grain size of Fe_3O_4-NPs was determined using the Scherrer equation, expressed as follows:

$$D = K.\frac{\lambda}{\beta}.\ cos\Theta$$

Where D is the crystallite size, K is the shape factor, λ is the X-ray wavelength, β is the line broadening at half maximum intensity (FWHM), and θ is the Bragg angle.

Figure 1B illustrates that the magnetite solution transitioned from bright yellow to dark brown, indicating that the metabolites in the aqueous extract of *A. cepa* may facilitate the reduction of Fe ions necessary for the formation of Fe_3O_4-NPs. The surface plasmon resonance (SPR) of Fe_3O_4 nanoparticles during the reaction period caused a color transition from bright yellow to dark; as illustrated in (Fig. 1B), the maximum wavelength of Fe3O4 nanoparticles was determined to be 372 nm.

Figure 2 illustrates the shape of the Fe_3O_4 nanoparticles synthesized by green methods. Figure 2B presents the ED results for Fe_3O_4 nanoparticles. Figure 2C illustrates the spherical morphology of the synthesized nanoparticles. Figure 3 revealed several spectral bands.

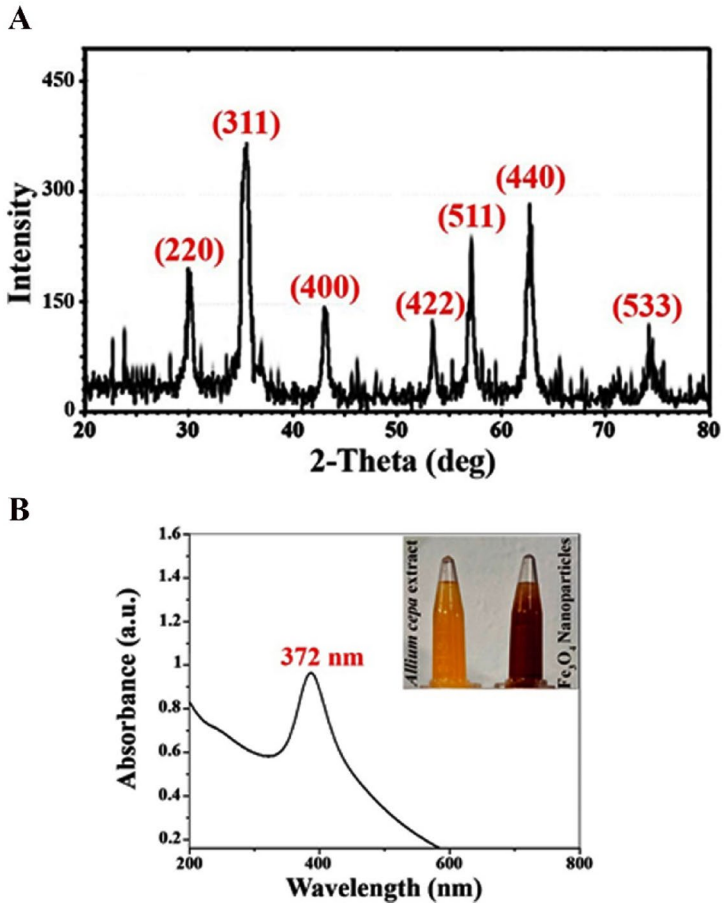

Fig. 1. XRD pattern of Fe_3O_4-NPs (**A**), UV-visible spectra of Fe_3O_4-NPs (**B**).

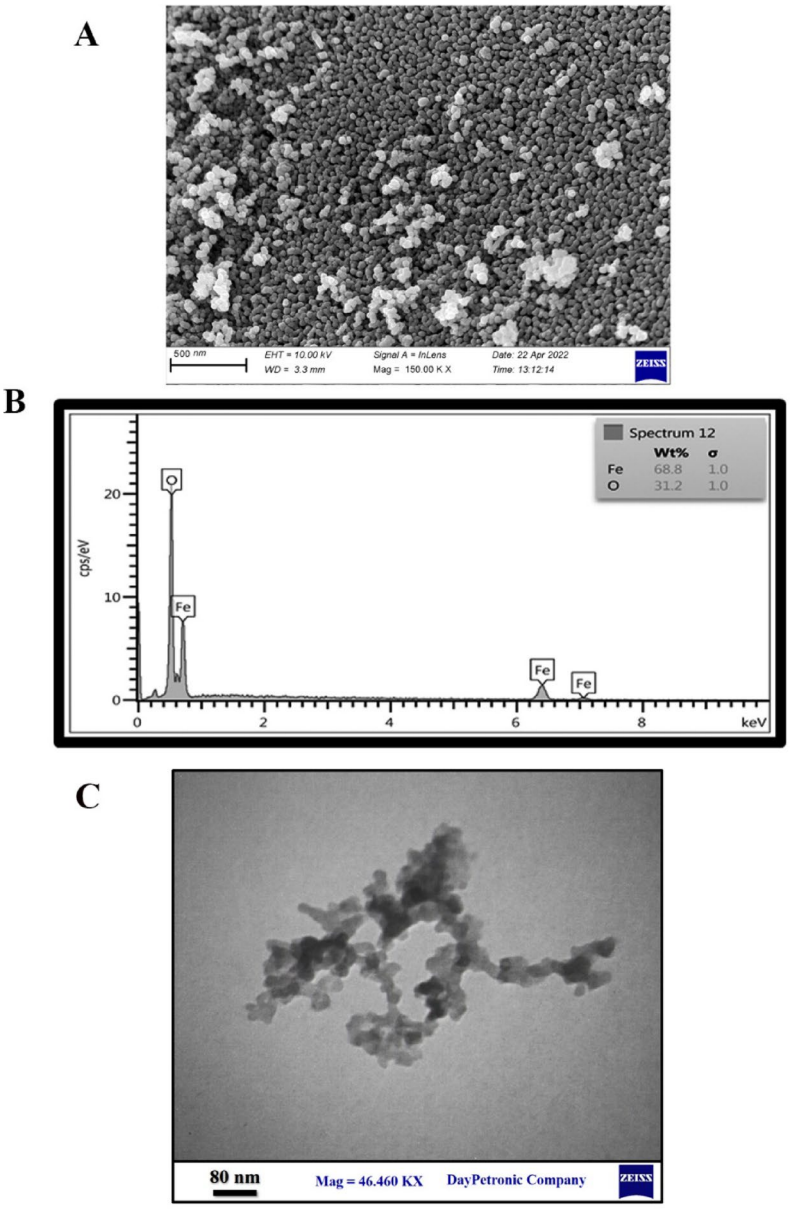

Fig. 2. Morphological characteristics of the nanoparticles: (**A**) Field emission scanning electron microscopy, (**B**) Energy dispersive spectroscopy, and (**C**) Transmission electron microscopy.

Antiviral activity of *A. cepa* extract and Fe_3O_4-NPs

The antiviral activity of *A. cepa* extract and prepared NPs is shown in (Fig. 4). The Fe_3O_4-NPs showed significantly higher cytotoxicity and neuraminidase enzyme inhibitory effects than the *A. cepa* extract; both effects happened in a dose-dependent manner. The generation of reactive oxygen species (ROS) was investigated using a flow cytometry assay as in Fig. 4 (Lower panel); the ROS generation by H1N1 influenza virus was increased, and after being treated with A. cepa extract and Fe_3O_4-NPs, the ROS generation was inhibited.

Antibacterial activity of *A. cepa* extract and Fe_3O_4-NPs

The bactericidal activity was evaluated; the Fe_3O_4-NPs exhibited markedly enhanced antibacterial activity against both S. aureus and E. coli, with the effect intensifying with rising concentrations, demonstrating a dose-dependent relationship, as illustrated in (Fig. 5).

Evaluation of both viable and non-viable bacterial strains

This work utilized acridine orange-ethidium bromide (AO/EtBr) staining to assess the viability of following treatment with the investigated agents, as illustrated in (Fig. 6). EtBr stain can only penetrate cells with compromised membrane integrity and interact with cellular nucleic acid. A green pigment denotes the living bacterium, but the deceased cells will exhibit a red stain[40]. In this study, *E. coli* and *S. aureus* treated with *A.*

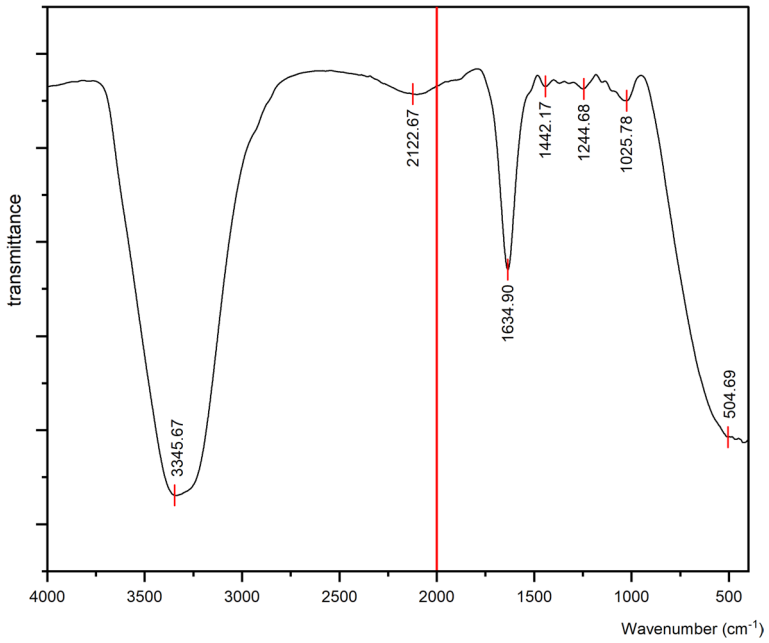

Fig. 3. Fourier transform infrared spectroscopy analysis of the green produced nanoparticles.

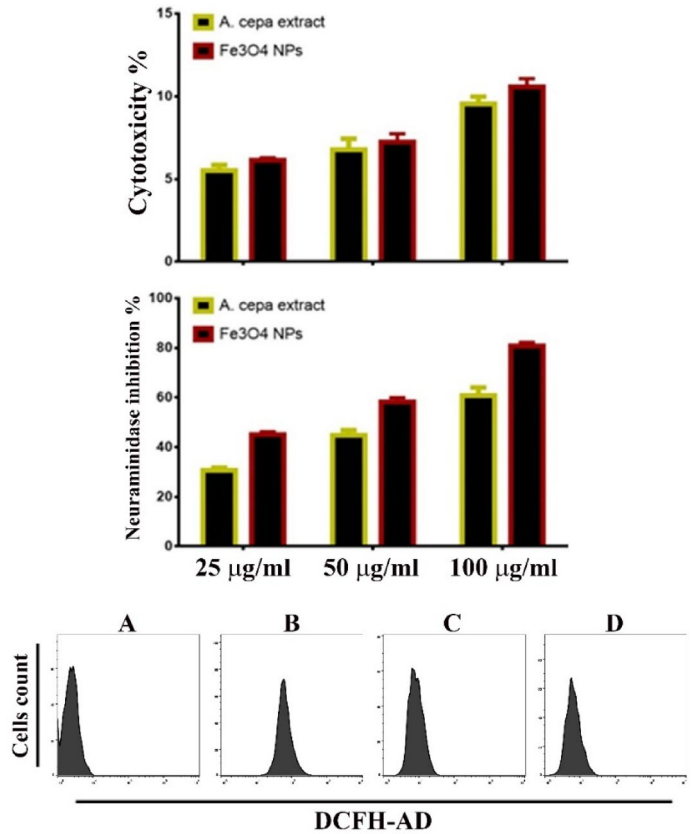

Fig. 4. Antiviral activity of *A. cepa* extract and Fe_3O_4-NPs. The upper panel represented the viability of MDCK cells after being treated with *A. cepa* extract and Fe_3O_4-NPs. The middle panel represented the ability of *A. cepa* extract and Fe_3O_4-NPs to inhibit neuraminidase enzyme. The concentration of Fe_3O_4-NPs was (25–100) µg/ml. Data were represented as mean ± SD of 3 independent experiments. The lower panel represented ROS generation assay using DCFH-AD. (**A**) Control untreated cells. (**B**) Cells were infected with the virus. (**C**) Cells infected with the virus in the presence of *A. cepa* extract. (**D**) Cells infected with the virus in the presence of Fe_3O_4-NPs at 50 µg/ml concentrations.

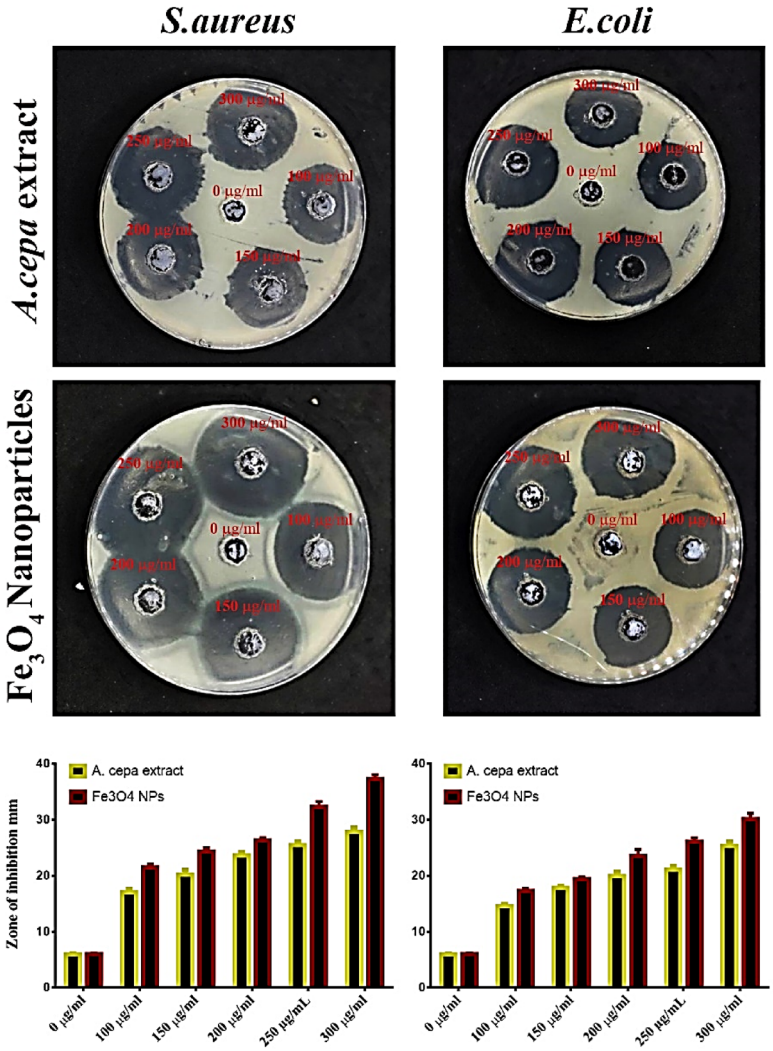

Fig. 5. Antibacterial efficacy of *A. cepa* extract with Fe_3O_4 nanoparticles against bacterial strains is demonstrated. The central well serves as a negative control. The concentration of Fe_3O_4-NPs was 100 to 300 µg/ml. Data were represented as mean ± SD of 3 independent experiments.

cepa extract and Fe_3O_4-NPs demonstrated compromised membrane integrity, resulting in increased molecular deformities and reduced bacterial counts. Conversely, untreated bacterial cells exhibited an entire, stable configuration and a vivid green stain.

A. cepa extract and Fe_3O_4-NPs induce oxidative stress

In this experiment, we assessed the bactericidal processes of *A. cepa* extract and Fe_3O_4-NPs. The DCFDA assay was used to measure the levels of ROS generation in *S. aureus* and E. *coli* after being treated with *A. cepa* extract and Fe_3O_4-NPs. When *S. aureus* and E. *coli* were treated with *A. cepa* extract and Fe_3O_4-NPs, the flow cytometry results showed a significant increase in ROS generation in comparison to untreated bacterial cells, as indicated in (Fig. 7). When compared to untreated bacterial cells, this treatment increased the number of S. aureus and E. coli cells that exhibited DCFDA (green fluorescence).

A. cepa extract and Fe_3O_4-NPs changed the bacterial membrane potential

Another antibacterial mechanism is believed to involve altering the cell membrane potential. Bacterial viability depends on membrane potential. The alteration of the membrane potential is therefore an early sign of bacterial damage. Rhodamine 123 dye was used in a flow cytometry assay to assess membrane potential in our study. When compared to untreated bacteria, both *S. aureus* and *E. coli* showed a significant decrease in mean fluorescence intensity (MFI) as indicated in (Fig. 8).

Antioxidant activity of *A. cepa* extract and Fe_3O_4-NPs

The present study measures the free radical scavenging activity of *A. cepa* extract and Fe_3O_4-NPs using the DPPH assay. Figure 9A represents the ability of Fe_3O_4-NPs in DPPH radical scavenging. The ability of Fe_3O_4-

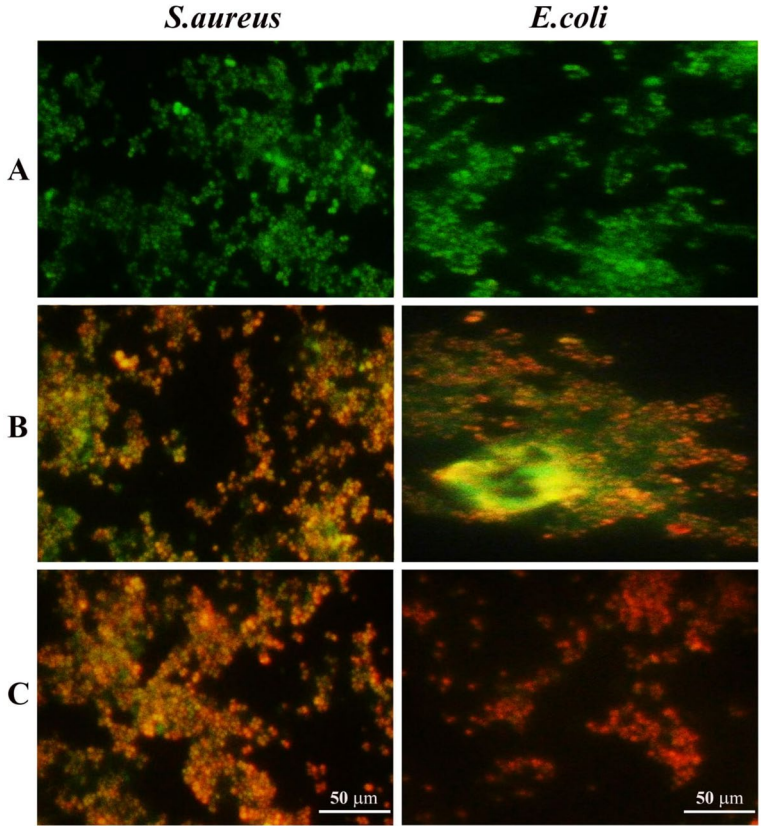

Fig. 6. Fluorescence microscopic images of the live and died bacteria. (**A**) Control untreated bacterial strains. (**B**) Bacterial strains treated with *A. cepa* extract at a 150 µg/mL concentration. (**C**) Bacterial strains treated with Fe_3O_4-NPs at concentration of 150 µg/mL Fe_3O_4-NPs.

NPs as radical scavengers is concentration-dependent. The Fe_3O_4-NPs scavenged more than 30% at lower concentrations. At the same time, the percentage was more than 80% at higher concentrations.

Figure 9B illustrates the antioxidant activity of *A. cepa* extract and Fe_3O_4-NPs using the ABTS assay. The increased *A. cepa* extract and Fe_3O_4-NPs concentrations improved ABTS radical scavenging abilities. The results show that the A. cepa extract and Fe3O4-NPs scavenged more than 70% ABTS free radicals at 200 µg/mL concentration.

A. cepa extract and Fe_3O_4-NPs induce phagocytosis

This experiment sought to evaluate the effect of pre-treatment with *A. cepa* extract and Fe_3O_4-NPs on the phagocytic capacity of BMDMs towards pH_{rodo} *E. coli* bioparticles. The present work demonstrates that *A. cepa* extract and Fe_3O_4-NPs boost the phagocytic and bactericidal capabilities of treated BMDM cells.

The capacity of BMDMs to phagocytose bacteria was examined through the absorption of tagged *E. coli* that could not release fluorescence till their translocation into the lysosome (low pH), as illustrated in (Fig. 10). The phagocytosis of pH_{rodo} E. coli bioparticles was studied after pre-treating BMDMs with *A. cepa* extract and Fe_3O_4-NPs at 25 µg/ml. The untreated control BMDM cells exhibited reduced phagocytic activity compared to those pretreated with *A. cepa* extract and Fe_3O_4-NPs BMDM cells.

We also aimed to test the mechanisms that could be involved in this process. The ability of BMDMs to phagocytose Candida albicans was tested. The results revealed that the ratio of cells that could phagocytose Candida albicans was significantly higher in the *A. cepa* extract and Fe3O4-NPs than in the BMDMs untreated cells ($p < 0.001$), as indicated in (Fig. 11).

Discussion

The rise of antibiotic-resistant strains as the foremost global public health issue underscores the need to discover new antibacterial compounds. Free iron ions and different metal and metal oxide nanoparticles, such as silver, ZnO, Al_2O_3, and TiO_2, have been evaluated as bactericidal or antibacterial agents[41–43]. Nonetheless, the primary issue associated with the utilization of nanoparticles exhibiting antibacterial characteristics is their elevated toxicity, as documented for ZnO[44,45]. In this context, iron oxide nanoparticles (IONPs) have recently emerged as an option owing to their bactericidal characteristics and biocompatibility in-vivo and in-vitro. Notwithstanding the promise of nanoparticles as antibacterial agents, certain dangers to human health and the environment have been documented. Conversely, IONPs have demonstrated safety and lack of toxicity in mammalian cell

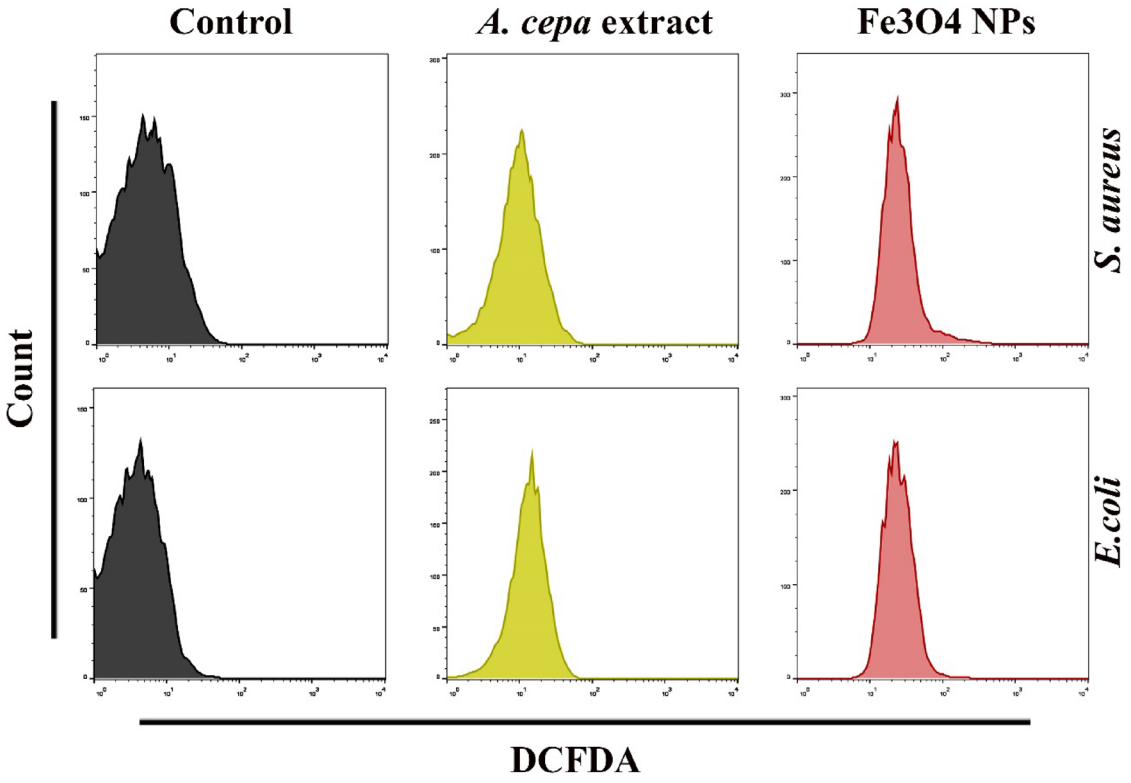

Fig. 7. *A. cepa* extract and Fe_3O_4-NPs induce ROS generation in *S. aureus* and *E. coli*.

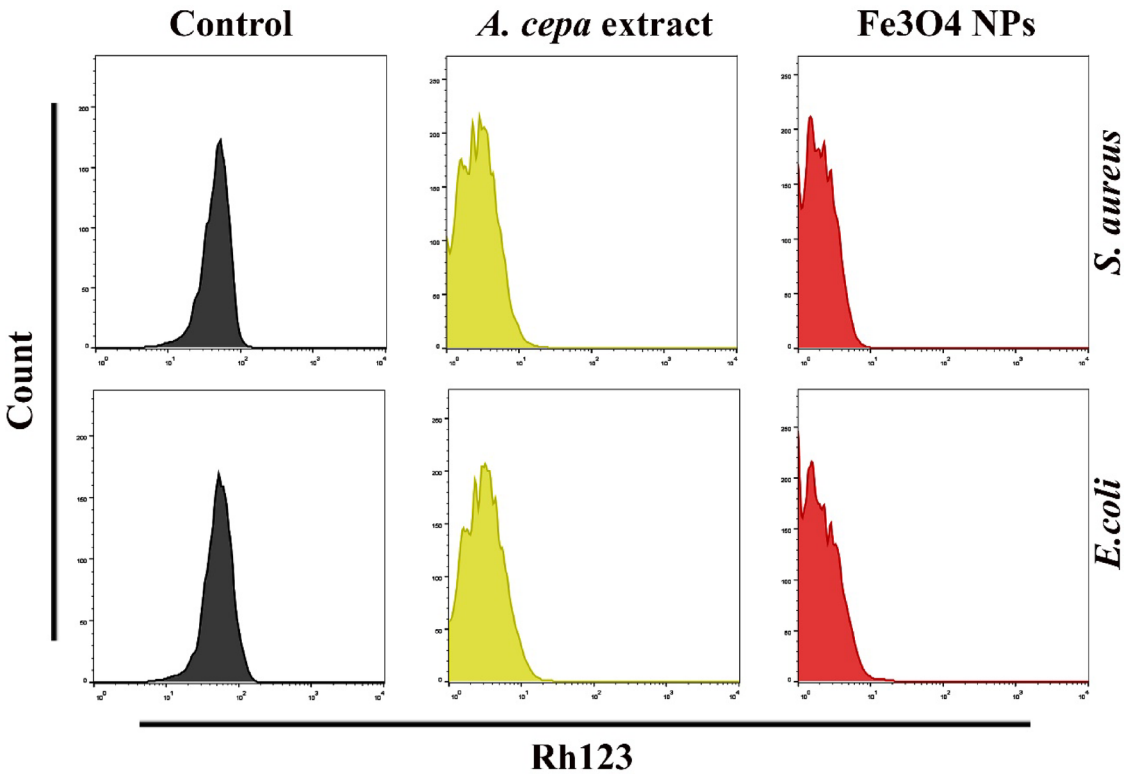

Fig. 8. *A. cepa* extract and Fe_3O_4-NPs altered the membrane potential of S. *aureus* and *E. coli*.

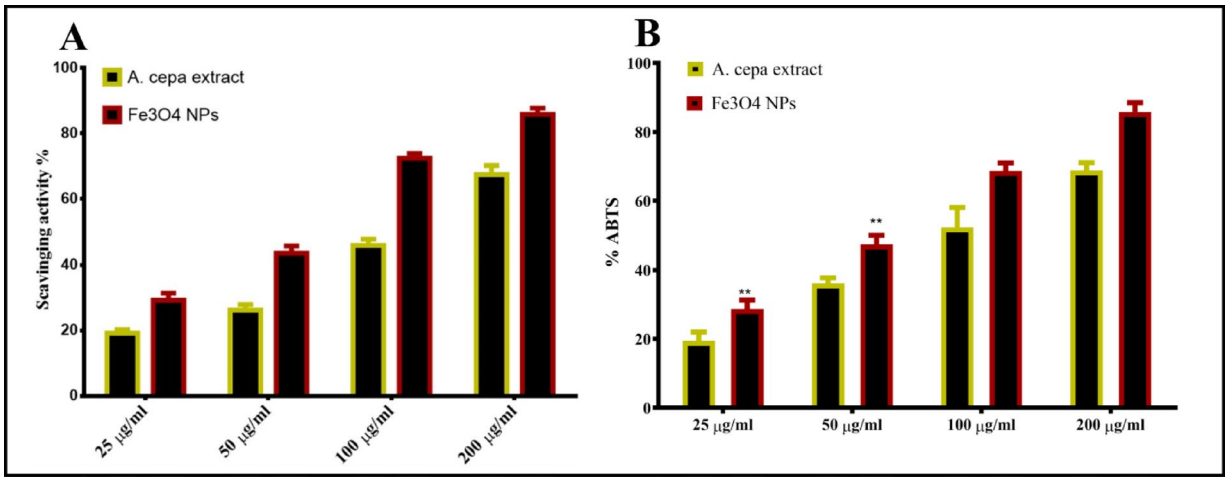

Fig. 9. Antioxidant activity of *A. cepa* extract and Fe_3O_4-NPs. (**A**) DPPH assay, (**B**) ABTS assay. The concentration of Fe_3O_4-NPs was 25–200 µg/ml. Data were represented as mean ± SD of 3 independent experiments.

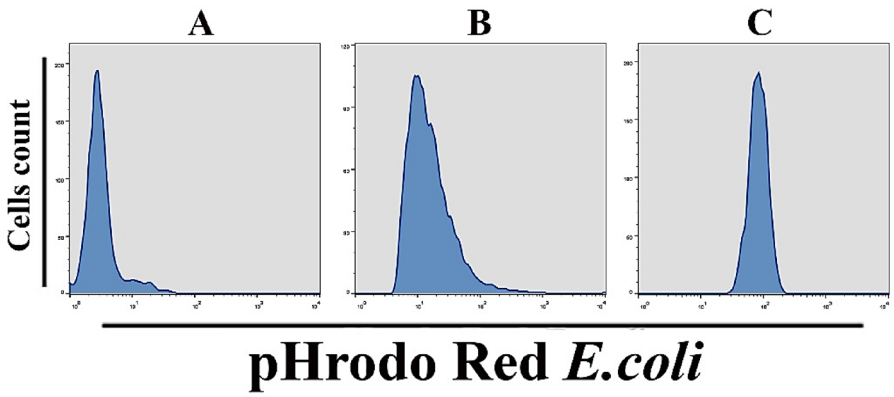

Fig. 10. *A. cepa* extract and Fe_3O_4-NPs augmented phagocytosis of pH_{rodo}*E. coli* bioparticles (**A**), BMDMs pretreated with pH_{rodo}*E. coli* bioparticles. (**B**) BMDMs were followed by pre-treatment with 25 µg/ml of *A. cepa* extract and then with pH_{rodo}*E. coli* bioparticles. (**C**) BMDMs were followed by pre-treatment with 25 µg/ml of Fe_3O_4-NPs and then with pH_{rodo}*E. coli* bioparticles.

cultures[46,47]. The most pertinent IONPs exhibiting biological activity are Fe_2O_3, magnetite Fe_3O_4, and limonite $Fe_2O_3{\cdot}H_2O$[48,49].

The current investigation demonstrated that the majority of the particles were agglomerated, perhaps attributable to the thickening capabilities of *A. cepa* or the presence of hydroxyl groups in the extract[50]. Furthermore, the propensity for agglomeration is expected given that the produced Fe3O4-NPs are compact in size and exhibit magnetic properties[51].

The morphological analysis of Fe3O4-NPs verifies the presence of clusters of spherical nanoparticles with sizes of 36 ± 1.23 nm. The findings indicated the existence of energy peaks for the Fe element at 0.8 KeV, 6.4 KeV, and 7 KeV, and for the oxygen element at 0.5 KeV. These findings corroborate the synthesis of Fe_3O_4, including 68.8% by weight of iron and 31.2% oxygen.

The O–H stretching vibration was suggested by the absorption peak of 3345.67 cm^{-1}. While 1634.90 cm^{-1} was attributed to the C-H bending overtone band of an aromatic compound[52]. While the peak at 1025.78 cm^{-1} was attributed to the C-O stretching band associated with the C-O-SO_3 group[53], the absorption peak at around 1244.68 cm^{-1} belonged to the asymmetric stretching vibration of the sulfate group[54]. FTIR spectrum of Fe_3O_4-NPs exhibited the presence of polyphenol in Fe_3O_4-NPs, showing its highest frequency at 504.69 cm^{-1}, corresponding to iron oxide nanoparticles.

The current study showed that *A. cepa* extract and Fe_3O_4-NPs had a potent inhibitory effect against the influenza virus. Furthermore, both showed a strong ability to diminish the activity of the viral neuraminidase enzyme. Onion possesses a substantial quantity of quercetin and flavonoid molecules, especially hesperetin, and can impede the intracellular replication of certain viruses, such as HIV[55,56]. Onion peels can reduce the degree of infection of subtype H9N2 both in vitro and in vivo[57].

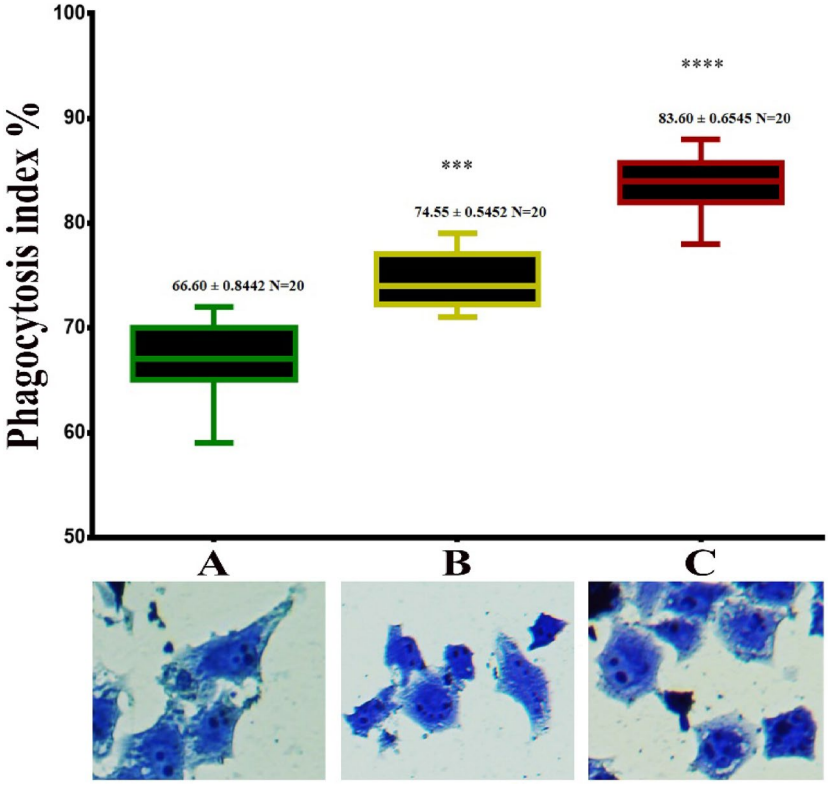

Fig. 11. *A. cepa* extract and Fe_3O_4-NPs increased Phagocytosis of *Candida albicans* by BMDMs. (**A**) The control group consisted of untreated BMDMs. (**B**) BMDMs following pre-treatment with 25 µg/ml of *A. cepa* extracT. (**C**) BMDMs following pre-treatment with 25 µg/ml of Fe_3O_4-NPs. Methylene blue was used to stain the macrophages. Data are represented as mean ± SD. Significant differences are shown at the level of $p < 0.001$ (***) and $p < 0.0001$ (****).

The flow cytometry assay showed that *A. cepa* extract and Fe_3O_4-NPs could reduce ROS generation in antiviral activity. Green synthesized palladium-NPs, Fe_3O_4-NP, and CuO-NPs were used as antiviral agents via four possible mechanisms: (1) direct viral interaction that prevents the virus from infecting the cells; (2) direct viral interaction that prevents the virus from entering the host cells; (3) blocking the virus's reproduction; or (4) additional processing mechanisms that prevent the virus from spreading[58].

The A. cepa extract and Fe3O4-NPs exhibited superior antimicrobial action towards the Gram-positive bacterial strain compared to the Gram-negative strain in the current investigation. Certain plant flavonoids, other natural compounds, and dietary supplements have exhibited antibacterial properties and the capacity to enhance the effectiveness of other antimicrobials[59]. Markiewicz et al. (2019)[60] studied the bactericidal potential of a polymer/Au/M-NPs nanohybrid that can successfully stop *Pseudomonas aeruginosa* metabolic activity and prevent biofilm formation. Due to the production of ROS, the majority of metal oxide nanoparticles have bactericidal effects[61]. According to the Fenton equations, the Fe^{2+} ions combine with the ROS species to create free hydroxyl radicals and hydrogen peroxide, which kills the bacteria[62]. Mesoporous silica nanoparticles (MSNPs) with a ligand (MSNPs-maleamic) and others with copper (III) coordination ions (MSNPs-maleamic-Cu) showed antibacterial action against *S. aureus* and *E. coli*. The antibacterial action of MSN-maleamic and MSN-maleamic-Cu is established by the fact that the (MSNPs-maleamic-Cu) significantly increased ROS in both species (30–50% more than in control untreated (MSNPs-maleamic-Cu) treated bacteria[63]. The findings of this study indicate that A. cepa extract and Fe_3O_4-NPs may enhance antibacterial efficacy against bacterial infections, thereby diminishing the demand for antimicrobial agents and improving efforts to prevent and manage bacterial resistance.

Moreover, the fluorescence microscopic images revealed that S. aureus and E. coli treated with A. cepa extract and Fe_3O_4-NPs compromised membrane integrity, resulting in increased molecular deformities and lowered bacterial counts. Conversely, untreated bacterial cells exhibited an entire, stable configuration and a vibrant green appearance. The results reveal that A. cepa extract and Fe_3O_4-NPs exert antibacterial effects by disrupting cell membrane integrity, suggesting a potential molecular basis for their action.

Many nanoparticles were used in numerous antibacterial investigations. The presence of ROS produced by various nanoparticles causes bactericidal action. The antibacterial activity of Fe_3O_4-NP may be due to a chemical reaction between hydrogen peroxide and membrane proteins or between the chemical generated in the presence of Fe_3O_4-NP and the bacterial outer bilayer. Bacteria are killed when the hydrogen peroxide generated penetrates their cell membrane. Additionally, it is seen that when hydrogen peroxide is produced, the nanoparticles remain

in contact with the dead bacteria, preventing them from acting further and continuing to manufacture and release hydrogen peroxide into the medium.

The current study results demonstrated that pre-treatment with *A. cepa* extract and Fe_3O_4-NPs increases the ability of phagocytosis; this suggests that the ability of BMDMs to kill microorganisms could be enhanced. As a result of oxidative metabolic activities and in reaction to endogenous signals like cytokines or exogenous signals like pathogens, ROS levels in cells are in a dynamic but stable equilibrium that is made up of the sum of all creating and removing components[64]. In addition to generating ROS, macrophages use various direct antimicrobial methods, such as delivering cathepsins and other hydrolases into mature phagosomes and producing reactive nitrogen species (RNS) within the phagosome[65]. For instance, the production of oxidative stress in phagocytes' pathogen-containing phagosomes is an essential part of antimicrobial immunity[66]. When macrophages identify bacteria, ROS are produced in various cellular compartments where they carry out various antimicrobial responsibilities. The inactivation of phagocytosed bacteria by the oxidative burst produced by Nox2 was one of the earliest functional roles for ROS produced by macrophages to be described. When invasive bacteria are recognized, a rapid and strong generation of ROS is released into the phagosomal lumen and extracellular ROS[67]. Mammalian sterile 20-like kinases 1/2 (MST1/MST2), two phagosome-located kinases that control mitochondrial recruitment to *Listeria monocytogenes* containing phagosomes, were discovered in the study of[67]. MST1/2-deficient BMDM demonstrated a higher bacterial burden and ROS generation into phagosomes. The mitochondrial contribution to phagosomal ROS levels was measured using *Escherichia coli* connected to the ROS probe CellROX. Notably, matrix mtROS levels remained unchanged, as assessed by MitoSOX, indicating that MST1/2 did not directly control mtROS generation. The generation of ROS from mitochondria or Nox2 is essential for antibacterial defense[68].

Conclusions

Green chemistry principles were employed in the synthesis of nanomaterials to produce beneficial substances and minimize waste products. The Fe_3O_4 nanoparticles were effectively synthesized utilizing the Iraqi onion peel fruit extract. Their characterization was validated, which revealed that the synthesized nanoparticles were spherical and uniform, measuring 36 nm. The nanoparticles demonstrate antiviral and antibacterial efficacy against S. aureus and E. coli. Antibacterial efficacy is ascribed to their capacity to produce reactive oxygen species, which induce oxidative stress and damage bacterial cells. The reactive oxygen species produced can provoke lipid peroxidation, protein oxidation, DNA damage, and membrane disruption in bacterial cells, resulting in their demise. Indicating the potential of the nanoparticles to serve as an efficient antibacterial and antioxidant agent. This study also indicated that A. cepa and Fe3O4-NPs significantly influence phagocytosis modulation. Ultimately, the current study's findings indicate that Fe_3O_4-NPs may serve as a potent antibacterial agent in several medicinal and biochemical applications.

Data availability

"Data are available upon request from the corresponding author."

Received: 16 December 2024; Accepted: 26 June 2025
Published online: 29 July 2025

References

1. Stiufiuc, G. F. & Stiufiuc, R. I. Magnetic nanoparticles: synthesis, characterization, and their use in biomedical field. *Appl. Sci.* **14** (4), 1623 (2024). https://www.mdpi.com/2076-3417/14/4/1623
2. Çiçek Özkul, S. L., Kaba, İ. & Ozdemir Olgun, F. A. Unravelling the potential of magnetic nanoparticles: a comprehensive review of design and applications in analytical chemistry. *Anal. Methods*. **16** (23), 3620–3640. https://doi.org/10.1039/D4AY00206G (2024).
3. Liu, L. et al. Green synthesis of Fe(3)O(4) nanoparticles using Alliaceae waste (Allium sativum) for a sustainable landscape enhancement using support vector regression. *Chemosphere* **334**, 138638 https://doi.org/10.1016/j.chemosphere.2023.138638 (2023).
4. Rezaei, B. et al. Magnetic nanoparticles: A review on synthesis, characterization, functionalization, and biomedical applications. Small (Weinheim an der Bergstrasse. *Germany)* **20** (5), e2304848. https://doi.org/10.1002/smll.202304848 (2024).
5. Mishra, S. & Yadav, M. D. Magnetic nanoparticles: A comprehensive review from synthesis to biomedical frontiers. *Langmuir* **40** (33), 17239–17269. https://doi.org/10.1021/acs.langmuir.4c01532 (2024).
6. Aminzai, M. T., Yildirim, M. & Yabalak, E. Metallic nanoparticles unveiled: synthesis, characterization, and their environmental, medicinal, and agricultural applications. *Talanta* **280** https://doi.org/10.1016/j.talanta.2024.126790 (2024).
7. Ogbezode, J. E., Ezealigo, U. S., Bello, A., Anye, V. C. & Onwualu, A. P. A narrative review of the synthesis, characterization, and applications of iron oxide nanoparticles. *Discov Nano*. **18** (1), 125. https://doi.org/10.1186/s11671-023-03898-2 (2023).
8. Khan, M., Khan, S., Omar, M., Sohail, M. & Ullah, I. Nickel and Cobalt magnetic nanoparticles (MNPs): synthesis, characterization, and applications. *J. Chem. Reviews*. **6** (1), 94–114. https://doi.org/10.48309/jcr.2024.419127.1274 (2024).
9. Nowak-Jary, J. & Machnicka, B. Comprehensive analysis of the potential toxicity of magnetic Iron oxide nanoparticles for medical applications: cellular mechanisms and systemic effects. *Int. J. Mol. Sci.* **25** (22). https://doi.org/10.3390/ijms252212013 (2024).
10. Ragab, A. H. et al. Exploring the sustainable synthesis pathway and comprehensive characterization of magnetic hybrid alumina nanoparticles phase (MHAl-NPsP) as highly efficient adsorbents and selective copper ions removal. *Environ. Technol. Innov.* **34**, 103628DOI. https://doi.org/10.1016/j.eti.2024.103628 (2024).
11. Kumari, S. et al. A comprehensive review on various techniques used for synthesizing nanoparticles. *J. Mater. Res. Technol.* **27**, 1739–1763. https://doi.org/10.1016/j.jmrt.2023.09.291 (2023).
12. Abid, N. et al. Synthesis of nanomaterials using various top-down and bottom-up approaches, influencing factors, advantages, and disadvantages: A review. *Adv. Colloid Interface Sci.* **300**, 102597DOI. https://doi.org/10.1016/j.cis.2021.102597 (2022).
13. Safat, S., Buazar, F., Albukhaty, S. & Matroodi, S. Enhanced sunlight photocatalytic activity and biosafety of marine-driven synthesized cerium oxide nanoparticles. *Sci. Rep.* **11** (1), 14734. https://doi.org/10.1038/s41598-021-94327-w (2021).
14. de Marco, B. A., Rechelo, B. S., Tótoli, E. G., Kogawa, A. C. & Salgado, H. R. N. Evolution of green chemistry and its multidimensional impacts: A review. *Saudi Pharm. Journal: SPJ : Official Publication Saudi Pharm. Soc.* **27** (1), 1–8. https://doi.org/10.1016/j.jsps.2018.07.011 (2019).

15. Kadhim, A. A. et al. Investigating the effects of biogenic zinc oxide nanoparticles produced using Papaver somniferum extract on oxidative stress, cytotoxicity, and the induction of apoptosis in the THP-1 cell line. *Biol. Trace Elem. Res.* **201** (10), 4697–4709. https://doi.org/10.1007/s12011-023-03574-7 (2023).
16. Ezeuko, A. S., Ojemaye, M. O., Okoh, O. O. & Okoh, A. I. Potentials of metallic nanoparticles for the removal of antibiotic resistant bacteria and antibiotic resistance genes from wastewater: A critical review. *J. Water Process. Eng.* **41**, 102041. https://doi.org/10.1016/j.jwpe.2021.102041 (2021).
17. Oladimeji, T. E. et al. Review on the impact of heavy metals from industrial wastewater effluent and removal technologies. *Heliyon* **10** (23), e40370. https://doi.org/10.1016/j.heliyon.2024.e40370 (2024).
18. Rathod, S., Preetam, S., Pandey, C. & Bera, S. P. Exploring synthesis and applications of green nanoparticles and the role of nanotechnology in wastewater treatment. *Biotechnol. Rep.* **41**, e00830. https://doi.org/10.1016/j.btre.2024.e00830 (2024).
19. Ali Abdul-Ameer, M. & Almousawy, N. A. *Growth and productivity of Onion (Allium cepa L.) as influenced by set size and spraying with Nanocarbon*. (IOP Publishing, 2019).
20. ChakrabortyAJ et al. Allium cepa: A treasure of bioactive phytochemicals with prospective health benefits. *Evid. Based Complement. Altern. Med. eCAM* **2022** 4586318 https://doi.org/10.1155/2022/4586318 (2022).
21. Stanisavljević, N. et al. Antioxidant and antiproliferative activity of Allium ursinum and their associated microbiota during simulated in vitro digestion in the presence of food matrix. *Front. Microbiol.* **11**, 601616DOI. https://doi.org/10.3389/fmicb.2020.601616 (2020).
22. Marefati, N. et al. A review of anti-inflammatory, antioxidant, and Immunomodulatory effects of Allium cepa and its main constituents. *Pharm. Biol.* **59** (1), 287–302. https://doi.org/10.1080/13880209.2021.1874028 (2021).
23. Chehregani, A., Azimishad, F. & Alizade, H. H. Study on antibacterial effect of some Allium species from Hamedan-Iran. *Int. J. Agric. Biol.* **9** (6), 873–876 (2007).
24. Kumar, V. P., Prashanth, K. V. H. & Venkatesh, Y. P. Structural analyses and Immunomodulatory properties of fructo-oligosaccharides from onion (Allium cepa). *Carbohydr. Polym.* **117**, 115–122. https://doi.org/10.1016/j.carbpol.2014.09.039 (2015).
25. Bouqellah, N. A., Mohamed, M. M. & Ibrahim, Y. Synthesis of eco-friendly silver nanoparticles using Allium sp. and their antimicrobial potential on selected vaginal bacteria. *Saudi J. Biol. Sci.* **26** (7), 1789–1794. https://doi.org/10.1016/j.sjbs.2018.04.001 (2019).
26. Iqbal, A. et al. Effects of Allium cepa-mediated zinc oxide nanoparticles on male reproductive tissue and sperm abnormalities of albino mice (Mus musculus). *Appl. Nanosci.* **11** (3), 807–815. https://doi.org/10.1007/s13204-020-01633-2 (2021).
27. Bale, V. K. & Reddy, K. H. Green synthesis, characterization and antimicrobial activity of nanosized cuprous oxide fabricated using aqueous extracts of Allium cepa and Raphanus sativus. *Int. J. Nano Dimension*. **13** (2), 214–226 (2022).
28. Win, T. T., Khan, S., Bo, B., Zada, S. & Fu, P. Green synthesis and characterization of Fe(3)O(4) nanoparticles using Chlorella-K01 extract for potential enhancement of plant growth stimulating and antifungal activity. *Sci. Rep.* **11** (1), 21996. https://doi.org/10.1038/s41598-021-01538-2 (2021).
29. Maded, Z. K. et al. Development and optimization of Dipyridamole- and Roflumilast-Loaded nanoemulsion and nanoemulgel for enhanced skin permeation: formulation, characterization, and in vitro assessment. *Pharmaceuticals* **17** (6). https://doi.org/10.3390/ph17060803 (2024).
30. Kaplan, A., Çiftçi, G. A. & Kutlu, H. M. Melatonin induces antiproliferative activity through modulation of apoptoticpathway in H-ras oncogene transformed 5RP7 cells. *Turkish J. Biology*. **39** (6), 879–887 (2015).
31. Dutta, S., Mitra, S. K., Bir, A. & Ghosh, T. R. P. Enhancing Anti-cancer activity: green synthesis and cytotoxicity evaluation of Turmeric-Gold nanocapsules on A549 lung Cancer cells. *Cureus* **15** (8), e43087. https://doi.org/10.7759/cureus.43087 (2023).
32. Ibraheem, H. H. et al. Insights into the pharmaceutical properties and in Silico study of novel hydrazone derivatives. *Sci. Rep.* **14** (1). https://doi.org/10.1038/s41598-024-81555-z (2024).
33. Ibraheem, D. R. et al. Nystatin-Based zinc oxide nanoparticles coated with polyethylene glycol for enhancing the antibacterial activity against some resistance pathogenic Bacteria. *BioNanoScience* https://doi.org/10.1007/s12668-024-01492-z (2024).
34. Paneth, A. et al. Synthesis and antibacterial evaluation of Mannich bases derived from 1,2,4-Triazole. *Chem. Biodivers.* **16** (10), e1900377. https://doi.org/10.1002/cbdv.201900377 (2019).
35. Ibraheem, D. R. et al. Nystatin-Based zinc oxide nanoparticles coated with polyethylene glycol for enhancing the antibacterial activity against some resistance pathogenic Bacteria. *BioNanoScience* **14** (3), 2103–2116. https://doi.org/10.1007/s12668-024-01492-z (2024).
36. Palau, M. et al. In vitro antibacterial activity of silver nanoparticles conjugated with Amikacin and combined with hyperthermia against Drug-Resistant and Biofilm-Producing strains. *Microbiol. Spectr.* **11** (3), e0028023. https://doi.org/10.1128/spectrum.00280-23 (2023).
37. Adeniji, O. O., Ojemaye, M. O. & Okoh, A. I. Antibacterial activity of metallic nanoparticles against Multidrug-Resistant pathogens isolated from environmental samples: nanoparticles/Antibiotic combination therapy and cytotoxicity study. *ACS Appl. Bio Mater.* https://doi.org/10.1021/acsabm.2c00527 (2022).
38. Sameen, A. M., Jabir, M. S. & Al-Ani, M. Q. Therapeutic combination of gold nanoparticles and LPS as cytotoxic and apoptosis inducer in breast cancer cells. *AIP Conf. Proc.***2213** (1) https://doi.org/10.1063/5.0000161 (2020).
39. Kadhim, R. J., Karsh, E. H., Taqi, Z. J. & Jabir, M. S. Biocompatibility of gold nanoparticles: In-vitro and In-vivo study. *Mater. Today Proc.* **42**, 3041–3045 https://doi.org/10.1016/j.matpr.2020.12.826 (2021).
40. Abbas, Z. S. et al. Galangin/β-Cyclodextrin inclusion complex as a Drug-Delivery system for improved solubility and biocompatibility in breast Cancer treatment. *Molecules (Basel Switzerland)* **27** (14). https://doi.org/10.3390/molecules27144521 (2022).
41. Slavin, Y. N., Asnis, J., Häfeli, U. O. & Bach, H. Metal nanoparticles: Understanding the mechanisms behind antibacterial activity. *J. Nanobiotechnol.* **15** (1), 65. https://doi.org/10.1186/s12951-017-0308-z (2017).
42. Majeed, S., Abdullah MSb, Nanda, A. & Ansari, M. T. In vitro study of the antibacterial and anticancer activities of silver nanoparticles synthesized from penicillium Brevicompactum (MTCC-1999). *J. Taibah Univ. Sci.* **10** (4), 614–620. https://doi.org/10.1016/j.jtusci.2016.02.010 (2016).
43. Saadh, M. J. et al. Metal nanoparticles as a promising therapeutic approach for prostate cancer diagnosis and therapy: a comprehensive review. *Med. Oncol.* **42** (4). https://doi.org/10.1007/s12032-025-02633-4 (2025).
44. Wang, L. et al. Recent advances on biosorption by aerobic granular sludge. *J. Hazard. Mater.* **357**, 253–270. https://doi.org/10.1016/j.jhazmat.2018.06.010 (2018).
45. Mathur, P., Saini, S., Paul, E., Sharma, C. & Mehtani, P. Endophytic fungi mediated synthesis of iron nanoparticles: characterization and application in methylene blue decolorization. *Curr. Res. Green. Sustain. Chem.* **4**, 100053. https://doi.org/10.1016/j.crgsc.2020.100053 (2021).
46. Li, D., Shen, M., Xia, J. & Shi, X. Recent developments of cancer nanomedicines based on ultrasmall iron oxide nanoparticles and nanoclusters. *Nanomed. (London England)*. **16** (8), 609–612. https://doi.org/10.2217/nnm-2021-0033 (2021).
47. Sihem, L., Hanine, D. & Faiza, B. Antibacterial activity of α-Fe2O3 and α-Fe2O3@Ag nanoparticles prepared by Urtica leaf extract. *Nanotechnol. Russ.* **15** (2), 198–203. https://doi.org/10.1134/S1995078020020135 (2020).
48. AlMatar, M., Makky, E. A., Var, I. & Koksal, F. The role of nanoparticles in the Inhibition of multidrug-resistant bacteria and biofilms. *Curr. Drug Deliv.* **15** (4), 470–484 (2018).

49. Ebrahiminezhad, A. et al. Biosynthesis of xanthangum-coated INPs by using Xanthomonas campestris. *IET Nanobiotechnol.* **12** (3), 254–258. https://doi.org/10.1049/iet-nbt.2017.0199 (2018).
50. Al-Karagoly, H. et al. Green synthesis, characterization, cytotoxicity, and antimicrobial activity of iron oxide nanoparticles using Nigella sativa seed extract. *Green. Process. Synthesis.* **11** (1), 254–265 (2022).
51. Ghosh, A., Srinivas, V., Kavita, S. & Sundara, R. Evolution of microstructure and magnetic properties from amorphous Fe3O4/SiO2 nanocomposite. *J. Magn. Magn. Mater.* **561**, 169687. https://doi.org/10.1016/j.jmmm.2022.169687 (2022).
52. Sri, S. P. S., Aron Santhosh Kumar, V., Savurirajan, Y. & Jha, M. Anticancer efficacy of magnetite nanoparticles synthesized using aqueous extract of brown seaweed Rosenvingea intricata, South andaman, India. *Sci. Rep.* **14** (1), 20255. https://doi.org/10.1038/s41598-024-67820-1 (2024).
53. Geneti, S. T. et al. Biogenic synthesis of magnetite nanoparticles using leaf extract of Thymus schimperi and their application for monocomponent removal of chromium and mercury ions from aqueous solution. *J. Nanomaterials.* **2022** (1), 5798824. https://doi.org/10.1155/2022/5798824 (2022).
54. Zhang, Z. et al. Synthesized oversulfated and acetylated derivatives of polysaccharide extracted from Enteromorpha linza and their potential antioxidant activity. *Int. J. Biol. Macromol.* **49** (5), 1012–1015. https://doi.org/10.1016/j.ijbiomac.2011.08.023 (2011).
55. Silva, J. L. et al. Red onion (Allium Cepa L.) methanolic extract increases extracellular nucleotide hydrolysis in rat serum. *Open. J. Appl. Sci.* **10** (12), 864–876 (2020).
56. Saadh, M. J. et al. Therapeutic effects of Quercetin in oral cancer therapy: a systematic review of preclinical evidence focused on oxidative damage, apoptosis and anti-metastasis. *Cancer Cell Int.* **25** (1). https://doi.org/10.1186/s12935-025-03694-1 (2025).
57. Kumar, M. et al. Onion (Allium Cepa L.) peels: A review on bioactive compounds and biomedical activities. *Biomed. Pharmacother.* **146**, 112498. https://doi.org/10.1016/j.biopha.2021.112498 (2022).
58. Bhatti, A. & DeLong, R. K. Nanoscale interaction mechanisms of antiviral activity. *ACS Pharmacol. Translational Sci.* **6** (2), 220–228. https://doi.org/10.1021/acsptsci.2c00195 (2023).
59. Alyamani, A. A. et al. Green fabrication of zinc oxide nanoparticles using Phlomis leaf extract: characterization and in vitro evaluation of cytotoxicity and antibacterial properties. *Molecules (Basel Switzerland)* **26** (20). https://doi.org/10.3390/molecules26206140 (2021).
60. Markiewicz, K. H. et al. Carbamohydrazonothioate-based polymer-magnetic nanohybrids: fabrication, characterization and bactericidal properties. *Arab. J. Chem.* **12** (8), 5187–5199. https://doi.org/10.1016/j.arabjc.2016.12.014 (2019).
61. Aisida, S. O. et al. Calcination induced PEG-Ni-ZnO Nanorod composite and its biomedical applications. *Mater. Chem. Phys.* **255**, 123603. https://doi.org/10.1016/j.matchemphys.2020.123603 (2020).
62. Touati, D. Iron and oxidative stress in bacteria. *Arch. Biochem. Biophys.* **373** (1), 1–6. https://doi.org/10.1006/abbi.1999.1518 (2000).
63. Díaz-García, D. et al. Preparation and study of the antibacterial applications and oxidative stress induction of copper Maleamate-Functionalized mesoporous silica nanoparticles. *Pharmaceutics* **11** (1). https://doi.org/10.3390/pharmaceutics11010030 (2019).
64. West, A. P. et al. TLR signalling augments macrophage bactericidal activity through mitochondrial ROS. *Nature* **472** (7344), 476–480. https://doi.org/10.1038/nature09973 (2011).
65. Mitchell, G., Chen, C. & Portnoy, D. A. Strategies used by Bacteria to grow in macrophages. *Microbiol. Spectr.* **4** (3). https://doi.org/10.1128/microbiolspec.MCHD-0012-2015 (2016).
66. Schramm, M. et al. Riboflavin (vitamin B2) deficiency impairs NADPH oxidase 2 (Nox2) priming and defense against Listeria monocytogenes. *Eur. J. Immunol.* **44** (3), 728–741. https://doi.org/10.1002/eji.201343940 (2014).
67. Herb, M. et al. Mitochondrial reactive oxygen species enable Proinflammatory signaling through disulfide linkage of NEMO. *Sci. Signal.* **12** (568). https://doi.org/10.1126/scisignal.aar5926 (2019).
68. Geng, J. et al. Kinases Mst1 and Mst2 positively regulate phagocytic induction of reactive oxygen species and bactericidal activity. *Nat. Immunol.* **16** (11), 1142–1152. https://doi.org/10.1038/ni.3268 (2015).

Acknowledgements

This work was supported by Ongoing Research Funding (ORF-2025-393), King Saud University, Riyadh, Saudi Arabia.

Author contributions

Conceptualization and methodology: AL-Salman HNK, Qasim QA, and Jabir MS; Formal analysis: Abbas BA, Hussein AJ, and Shari FH; Investigation, data curation, and visualization: Fawzi HA and Jabir MS; Writing—original draft preparation: AL-Salman HNK, Qasim QA, Abbas BA, Hussein AJ, Shari FH, Jabir MS, Gatasheh MK, AL-Farga A, and Fawzi HA, Writing—review and editing: AL-Salman HNK, Qasim QA, Abbas BA, Hussein AJ, Shari FH, Jabir MS, Gatasheh MK, AL-Farga A, and Fawzi HA, Supervision: Jabir MS. All authors approved the final version of the manuscript.

Funding

"This work was supported by Ongoing Research Funding (ORF-2025-393), King Saud University, Riyadh, Saudi Arabia."

Declarations

Competing interests

The authors declare no competing interests.

Additional information

Correspondence and requests for materials should be addressed to M.S.J., M.K.G. or H.A.F.

Reprints and permissions information is available at www.nature.com/reprints.

Publisher's note Springer Nature remains neutral with regard to jurisdictional claims in published maps and institutional affiliations.